Batteries & Supercaps

Research Article
doi.org/10.1002/batt.202100408

Chemistry Europe
European Chemical Societies Publishing

www.batteries-supercaps.org

Building a House for Stabilizing Lithium-Metal Anodes

Lei You,[a] Jianwen Liu,[a] Hongyu Zhang,[b] Tianren Zhang,[d] Juan Wang,[d] Zaiping Guo,*[c] Guanglin Xia,*[b] and Xuebin Yu*[b]

Lithium (Li) metal is regarded as one of the most promising anode candidates for future high energy density lithium batteries. The practical application of Li-metal anodes, however, is hindered by the uncontrollable growth of dendrites resulting from both huge volume change and unstable solid-electrolyte interfaces upon cycling. Herein, we propose a novel "house strategy" that utilizes the 3D NiO nanosheets decorated nickel foam as the frame to confine Li metal and the inorganic $[LiNBH]_n$ chains with high Li ion conductivity as the artificial protective proof to establish a stable dendrite-free Li metal anode. Benefiting from the synergistic effect of the 3D NiO/Ni foam in lowering the local current density and accommodating the huge volume change of Li metal and the $[LiNBH]_n$ protective layer in facilitating uniform Li^+ diffusion and regulating Li deposition beneath this layer, the LiNBH-Li@Ni electrode presents an excellent long-term cycling lifespan of over 800 h at both 1 and 3 mA cm^{-2} with a high areal capacity of 5 mAh cm^{-2} in symmetric cells. Upon coupling this anode with $LiFePO_4$ cathode, the thus-assembled full cells deliver an ultrahigh reversible capacity of 127.4 mAh g^{-1} at 1 C after 200 cycles.

Introduction

Due to the increasing demand for high-energy-density storage devices of today's society, lithium (Li) metal has been widely regarded as the most competitive anode material applied in future high energy density lithium-ion batteries due to its ultrahigh theoretical capacity of 3860 mAh g^{-1}, the lowest redox potential (−3.04 V vs. the standard hydrogen electrode), and the comparatively light weight (0.53 g cm^{-3}).[1,2] The commercial application of Li metal anodes, however, has been seriously hindered by the uncontrollable growth of Li dendrites, resulting from the large volume change of Li metal and the unstable solid-electrolyte interfaces.[3,4] Particularly, the high chemical reactivity between Li and electrolyte results in the formation of fragile solid-electrolyte interphases (SEI) and the continuous consumption of both electrolyte and Li metal due to the easy destruction of fragile SEI layers induced by the large volume change of Li metal during repeated Li plating/stripping processes. Together, these phenomenon leads to continuous decay of coulombic efficiency and hence poor cycling stability of Li metal anodes.[5–7] More importantly, serious safety hazards could be caused due to the massive formation of Li dendrites, which may piece through the separator and trigger short circuit inside of the batteries.[8,9]

Accordingly, two major strategies have been developed to improve the stability of Li metal anodes via suppressing the growth of Li dendrites. The first one could be concluded as interfacial engineering via building artificial SEI layers through various *in-situ* or *ex-situ* strategies.[10–15] The uniform coating of artificial SEI layers could not only enhance the mechanical strength of SEI due to the high mechanical modulus of the artificial layers and suppress severe side reactions between Li metal and electrolyte, but also homogenize Li-ion flux distribution towards uniform Li deposition, contributing to the enhancement of the interfacial stability of Li metal anodes. In this aspect, a recent study in our group has validated that the fabrication of $[LiNBH]_n$ films with high Li ion conductivity as the artificial SEI layers effectively regulates the homogeneous distribution of Li-ion flux induced by the high polarity of $[LiBNH]_n$, leading to the deposition of Li underneath this layer, and suppress the corrosion of Li metal by the electrolyte, which effectively improves the cycling stability of Li-metal anodes.[16] Despite this progress, the electrochemical performance of Li metal anodes modified via building artificial SEI layers still fall short in efficiency and long-term stability for practical applications attributed to the infinite relative volume change of Li metal anode owing to its hostless nature during Li stripping/plating process. Therefore, confining Li into three-dimensional hosts (e.g., 3D copper/nickel foam,[17–22] 3D nanostructured carbon,[23–27] etc.) has been considered as an effective way for mitigating the large volume expansion of Li metal anodes. In addition, the conductive frameworks of 3D scaffolds are also

[a] L. You, Dr. J. Liu
Hubei Collaborative Innovation Center for Advanced Organic Chemical Materials
Ministry-of-Education Key Laboratory for Synthesis and Applications of Organic Functional Molecules
College of Chemistry and Chemical Engineering
Hubei University
Hubei 430062, China
[b] Dr. H. Zhang, Prof. G. Xia, Prof. X. Yu
Department of Materials Science
Fudan University
Shanghai 200433, China
E-mail: xiaguanglin@fudan.edu.cn
yuxuebin@fudan.edu.cn
[c] Prof. Z. Guo
School of Chemical Engineering & Advanced Materials
The University of Adelaide
Adelaide, SA 5005, Australia
E-mail: zaiping.guo@adelaide.edu.au
[d] Dr. T. Zhang, Dr. J. Wang
Zhejiang Tianneng Battery Co., Ltd.
Changxing 313100, Zhejiang, China

Supporting information for this article is available on the WWW under https://doi.org/10.1002/batt.202100408

Research Article
doi.org/10.1002/batt.202100408
Chemistry Europe
European Chemical Societies Publishing

capable of dissipating the current density uniformly on the surface of the electrode, which could effectively alleviate the growth of Li dendrites by reducing the local current density according to the Sand's time model.[28] Unfortunately, due to the lack of protection over Li metal located on the surface of the anode, the inevitable growth of Li dendrites on the surface of Li metal anode confined into these 3D hosts could still be observed upon the long-term Li stripping and plating process. It would eventually lead to the formation of "dead Li" upon cycling, accompanied with low coulombic efficiencies, and even battery failure. Therefore, it is still a great challenge to achieve long-term cycling stability of Li metal anodes.

In this work, we propose and demonstrate a "house strategy" to design a stable Li metal anode via confining Li metal into 3D Ni foams to alleviate the volume change of Li metal followed by in-situ formation of polymer-like $[LiNBH]_n$ chains as the protective roof for protecting Li metal located on the surface of the electrode from the corrosion of the electrolyte (denoted as LiNBH-Li@Ni). As illustrated in Figure 1(a), molten Li is infiltrated into lithiophilic 3D conductive Ni foams modified uniformly with NiO nanosheets (denotated as Li@Ni), which could not only facilitate rapid electron and ion transport through the interconnected frameworks with sufficient void spaces but also alleviate the large volume variation during the repeated Li stripping and plating process. In addition, the high lithiophilicity of Ni foams achieved by the homogeneous decoration with NiO nanosheets is able to regulate the uniform Li-deposition process, which contributes to suppressing the formation of Li dendrites. Subsequently, in order to protect Li metal located on the surface of Li@Ni from the corrosion of the electrolyte, a protective roof composed of crosslinked $[LiNBH]_n$ chains with high Li ion conductivity is homogeneously built on the surface of Li@Ni via in-situ reaction between Li and ammonia borane followed by facile thermal heating. Moreover, the high ionic conductivity and poor electronic conductivity of the thus-formed $[LiNBH]_n$ chains is capable of promoting uniform Li deposition underneath this artificial SEI layers, which hence suppresses the parasitic reaction on the surface of Li metal and benefits the formation of stable interfaces between the electrode and the electrolytes, hindering the formation of

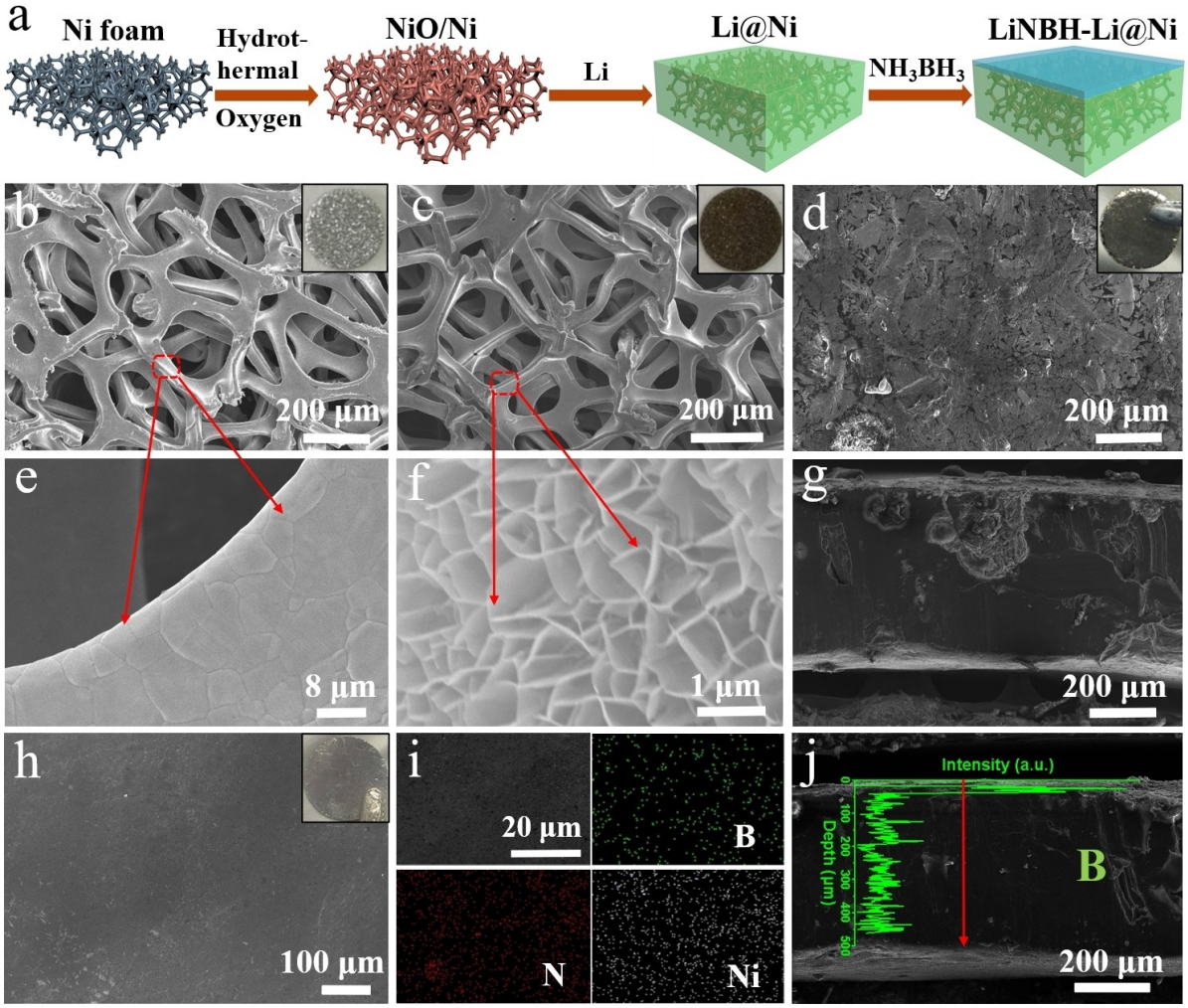

Figure 1. a) Schematic illustration for the synthesis process of the LiNBH-Li@Ni electrode. b, e) SEM images of Ni foams. c, f) SEM images of Ni foams uniformly decorated with NiO nanosheets. d) Top and g) cross-sectional SEM images of the thus-formed Li@Ni electrode. h) SEM image, i) EDS elemental mapping, and j) cross-sectional SEM image and EDS linear scanning profile of the thus-formed LiNBH-Li@Ni electrode.

Research Article
doi.org/10.1002/batt.202100408
Chemistry Europe
European Chemical Societies Publishing

Li dendrites and "dead Li". Based on the synergistic roles of these unique characteristics, the thus-fabricated LiNBH-Li@Ni electrode exhibits a long-term cycling performance over 800 h at a high current density of 3 mA cm^{-2} under a deep stripping/plating capacity of up to 5 mAh cm^{-2}. Impressively, upon coupling LiNBH-Li@Ni anode with a $LiFePO_4$ cathode, the thus-formed full cell displays an extremely high reversible capacity of 127.4 mAh g^{-1} after 200 cycles. These results demonstrate the potential of "house strategy"-design principle as an effective method for stabilizing Li-metal anodes towards practical applications.

Results and Discussion

As illustrated in Figure 1(a), the LiNBH-Li@Ni electrode is fabricated via the melt infiltration of Li metal into Ni foams followed by the uniform coating of $[LiNBH]_n$ chains through in-situ reaction between Li metal and ammonia borane after thermal heating. SEM images illustrate that the Ni foam cleaned by diluted hydrochloric acid exhibit a typical 3D porous skeleton with smooth surface (Figure 1b and e), possessing pore sizes ranging from 200 to 300 μm, which provides sufficient void spaces for subsequent melt infiltration of molten Li. Unfortunately, no obvious infiltration of molten Li into Ni foams could be observed for pure Ni foams (Movie S1), indicating their lithiopholic nature. Therefore, in order to improve the lithiophilic property of Ni foams, Ni foams are uniformly decorated with NiO nanosheets, which could be facile realized through a facile hydrothermal treatment with distilled water followed by heat-treatment in the air. After the thermal treatment process, the 3D structure of Ni foams is well maintained (Figure 1c) and uniform NiO nanosheets with a thickness of approximately 100 nm are vertically and homogeneously grown on the surface of the Ni skeletons as evidenced by the XRD patterns (Figure S1) and SEM image (Figure 1f), which turns the color of Ni foams from silver to dark brown (inset of Figure 1c). Interestingly, after modification with NiO nanosheets, the spontaneous infiltration of molten Li into Ni foam could be clearly observed upon contacting Ni foam with molten Li within the period of less than 10 seconds (Movie S2). The thus-formed electrode (denoted as Li@Ni) exhibits the typical metallic luster of Li after the melt infiltration process, demonstrating the good lithophilic nature of the Ni foam modified with NiO nanosheets, which could be attributed to the favorable reaction between NiO and Li with a negative Gibbs free energy.[29] As a result, metallic Li is uniformly space-confined into the void spaces of Ni framework (Figure 1d) and the thickness of the thus-obtained Li@Ni electrode, which exhibits the characteristic diffraction peaks of Li in XRD results (Figure 2a), is about 460 μm (Figure 1g). By calculating the weight change before and after Li infiltration, the areal mass loading of Li inside of Li@Ni electrode is calculated to be approximately 26 mg cm^{-2}, accounting for 48.1% of the total mass of the whole electrode.

Subsequently, in order to further suppress the continuous corrosion of Li metal located on the surface of Li@Ni anode by electrolyte, a protective roof composed of the polymer-like $[LiNBH]_n$ chains is homogeneously constructed on the surface of Li@Ni (denoted as LiNBH-Li@Ni electrode) using *in-situ*

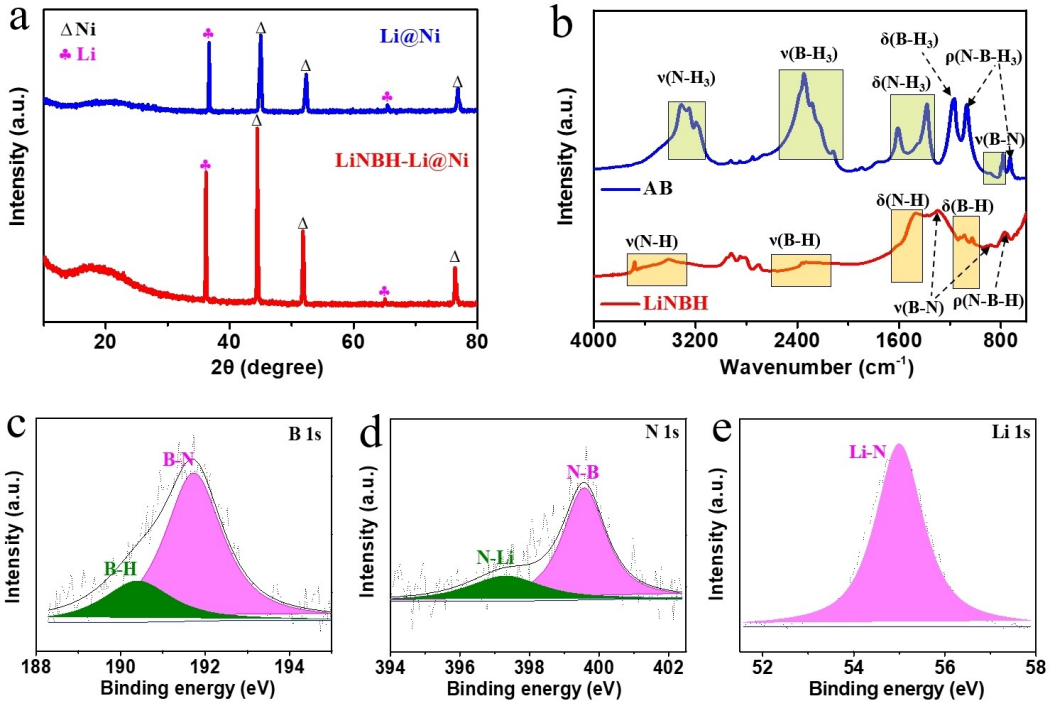

Figure 2. a) XRD pattern of the thus-formed Li@Ni and LiNBH-Li@Ni electrode. b) FTIR spectra of the NH_3BH_3 (AB) and the $[LiNBH]_n$ layer covered on the surface of the LiNBH-Li@Ni electrode. High-resolution XPS spectra of c) B 1s, d) N 1s, and e) Li 1s of the thus-formed LiNBH-Li@Ni electrode.

reaction between Li and ammonia borane (AB) followed by thermal heating. It is interesting to note that, although no extra peak of $[LiNBH]_n$ could be observed in the XRD results of the LiNBH-Li@Ni electrode due to its amorphous nature, the relative intensity of Li diffraction peaks in comparison with Ni peaks of the LiNBH-Li@Ni electrode is much lower than that of Li@Ni electrode (Figure 2a), which could be attributed to the consumption of Li metal during the formation of $[LiNBH]_n$ layers covered on the surface of the electrode. Therefore, Fourier-transform infrared (FTIR) spectra is further conducted to validate the successful synthesis of $[LiNBH]_n$ layers in detail. As shown in Figure 2(b), after the reaction of Li and ammonia borane followed by thermal annealing, the characteristic peaks of both N–H_3 and B–H_3 groups of ammonia borane disappear owing to the interaction of B–H and N–H bonds for hydrogen desorption accompanied by the significant increase of B–N bonds, which directly demonstrating the successful formation of polymer-like $[LiNBH]_n$ protective layer through the interaction between B–N and N–H bonds.[30,31] The chemical composition of the thus-formed $[LiNBH]_n$ layers is further investigated by X-ray photoelectron spectroscopy (XPS). The high-resolution B 1s spectrum (Figure 2c) exhibits tow typical peaks at 190.3 and 191.8 eV that could be indexed to B–H and B–N bonds of $[LiNBH]_n$, respectively, and two major peaks at 397.1 and 399.2 eV in the spectra of N 1s (Figure 2d) could be indexed to N–Li and N–B bonds of $[LiNBH]_n$,[16,32] which provides additional evidence to the formation of $[LiNBH]_n$. Interestingly, there is only one peak assigned to Li–N bond of $[LiNBH]_n$ at 54.9 eV in the spectrum of Li 1s (Figure 2e), and no characteristic peaks of metallic Li (Li^0) could be observed, directly demonstrating the uniform coating of $[LiNBH]_n$ on the surface of Li@Ni. In addition, the presence of strong and numerous Li–N ionic bonds between various $[LiNBH]_n$ chains results in a flexible polymer-like structure, which could not only alleviate the corrosion of Li metal by electrolyte, but also mitigate the volume change of Li metals located on the surface of the electrode. SEM measurement is adopted to visually characterize the formation of $[LiNBH]_n$ on the surface of Li@Ni electrode. As shown in Figure 1(h), in comparison with the Li@Ni anode, the surface of LiNBH-Li@Ni is smoother and more uniform due to the homogeneous coverage of $[LiNBH]_n$ layers (Figure 1h). The energy dispersive X-ray (EDS) elemental mapping results (Figure 1i) confirm the uniform distribution of the elemental B, N, and Ni on the surface of the electrode, indicating the homogeneous distribution of $[LiNBH]_n$ on the surface of LiNBH-Li@Ni. Moreover, according to the cross-sectional image and the corresponding EDS linear scanning analysis (Figure 1j), although the thickness of the LiNBH-Li@Ni electrode is comparable to that of Li@Ni electrode, the corresponding signal of element B could be detected only on the top layer of the electrode, which provides direct evidence for the uniform coating of $[LiNBH]_n$ layer on the surface of the electrode. The energy density of LiNBH-Li@Ni electrode was evaluated by galvanostatic charging method (Figure S2), which exhibits a high specific capacity of 1280.8 $mAh\,g^{-1}$.

The Li plating behavior of the LiNBH-Li@Ni electrode is subsequently investigated through in-situ optical microscopy visualization, with pristine Li metal and Li@Ni included for comparison. These studies were performed in transparent glass cell viewed by an electron optical microscopy (as schematically illustrated in Figure S3). As shown in Figure 3(a), numerous Li dendrites quickly arise and continue to radioactively grow on the surface of bare Li foil upon the proceeding of Li plating process due to the heterogeneous deposition of Li ions. After Li plating for only 10 min, the length of Li dendrites could reach more than 220 μm. In the term of Li@Ni electrode, although the conductive 3D Ni foams could dissipate the current density uniformly on the surface of the electrode to some extent, which could slow down the growth of Li dendrites by reducing the local current density, the massive growth of mossy Li with a thickness of over 100 μm could be clearly observed on the surface of the Li@Ni anode upon increasing the deposition time to 10 min (Figure 3b). In sharp contrast, the LiNBH-Li@Ni electrode displays a relatively flat and dense surface during the whole Li deposition process without the observation of any dendritic structure (Figure 3c). More importantly, the thickness of the top surface covered on the LiNBH-Li@Ni electrode is nearly constant after 10 min of Li plating process, indicating the inward Li deposition process induced by the uniform coating of $[LiNBH]_n$ layers with high Li ion conductivity, which promotes fast Li ion transport across the surface of the electrode towards stable Li plating process. This result directly demonstrates that the conductive 3D Ni frameworks and the uniform coating of $[LiNBH]_n$ layers of the LiNBH-Li@Ni electrode play a synergistic role in enhancing the Li plating stability of Li metal anodes.

To unravel the mechanism of $[LiNBH]_n$ layers with high Li ion conductivity in regulating the homogeneous Li plating process, dynamic simulation of Li deposition behavior is performed at a current density of 1 $mA\,cm^{-2}$ to simulate the distribution of electric field and Li ion according to finite element method using COMSOL Multiphysics. Two simulation cells are built, in which the LiNBH-Li@Ni model is modified with artificial $[LiNBH]_n$ layers with a high ionic conductivity of 0.66×10^{-5} $S\,cm^{-1}$[16] and the Li@Ni model is modified with a natural SEI layer with a low ionic conductivity of 1×10^{-9} $S\,cm^{-1}$.[33] Owing to the low Li ion conductivity of natural SEI layers, which impedes the transport of Li ions across the whole electrode, continuous accumulation of Li ions could be clearly observed on the top of the SEI layer of the Li@Ni electrode during Li plating process (Figure 3d), which directly causes a sharp increase of the potential gradient around the SEI layer (Figure 3f). As a result, the electrons are preferred to gather in regions with strong magnetic fields based on the "lightning rod theory",[34] thus leading to the uneven Li deposition on the top of the electrode and the formation of Li dendrites. On the contrary, the protective layers composed of $[LiNBH]_n$ chains with high Li ion conductivity could significantly alleviate the accumulation of Li ions on the top of the LiNBH-Li@Ni anode and facilitates the uniform dispersion of Li ion flux across the whole electrode (Figure 3e). Coupled with an extremely homogeneous potential distribution across the whole LiNBH-Li@Ni anode (Figure 3g), the design of a house with electronic conductive 3D Ni foams as the hosts and the $[LiNBH]_n$ layers

Research Article
doi.org/10.1002/batt.202100408
Chemistry Europe
European Chemical Societies Publishing

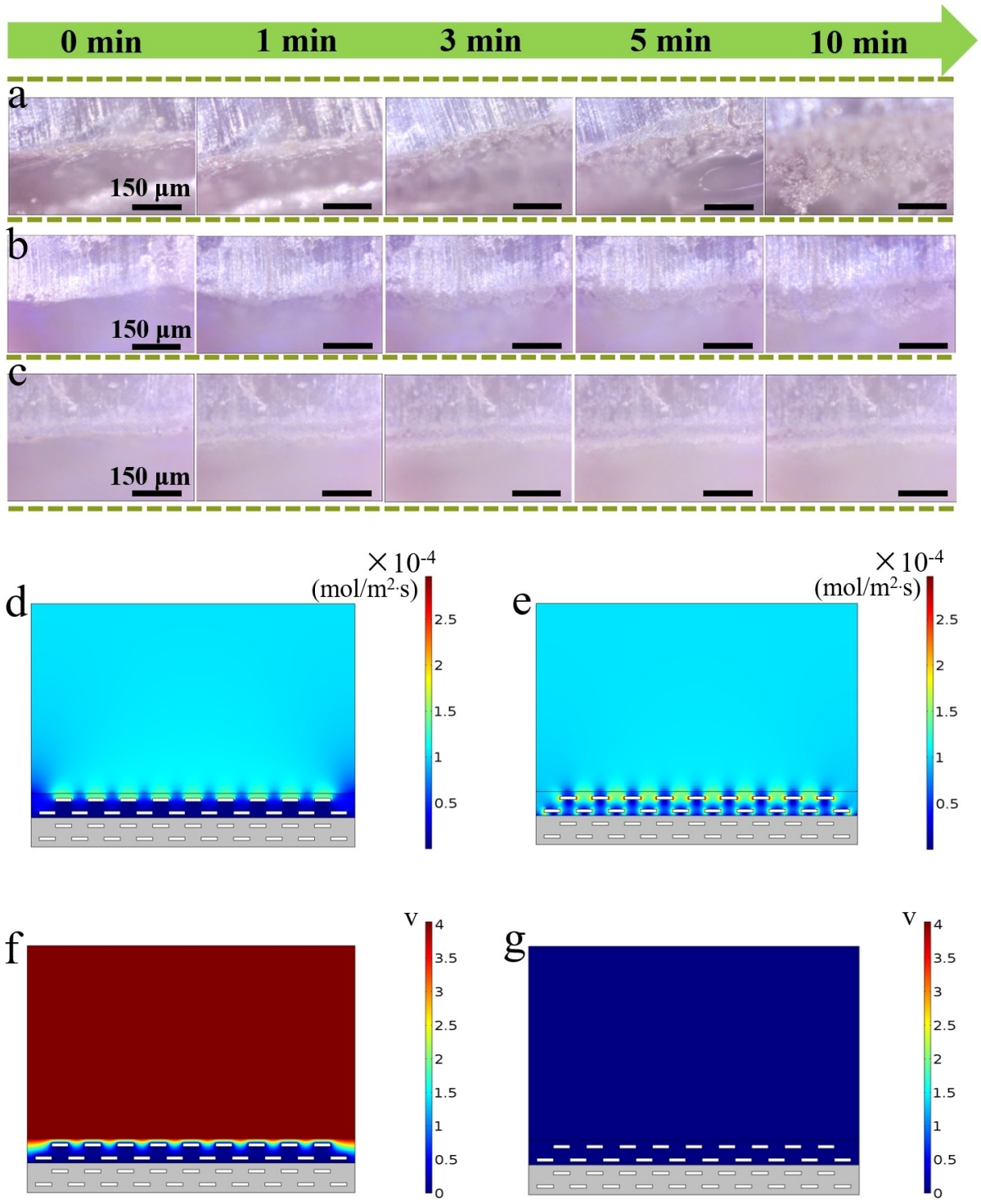

Figure 3. In situ optical microscopy visualization of Li electrodeposition process on a) bare Li, b) Li@Ni, and c) LiNBH-Li@Ni at a current rate of 5 mA cm^{-2} after various times. Finite element simulations of lithium flux and potential distribution on d, f) Li@Ni and e, g) LiNBH-Li@Ni electrode.

with high Li ion conductivity as the protective roof could effectively promote the Li deposition underneath the $[LiNBH]_n$ layers and hence retard the growth of Li dendrites.

To evaluate the electrochemical performance of the LiNBH-Li@Ni electrode, symmetric cells are subsequently assembled and tested under various current densities and cycling capacities, with Li@Ni and bare Li electrodes included for comparison. Upon cycling at 1 mA cm^{-2} with a fixed areal capacity of 1 mAh cm^{-2}, a clear increase of overpotential could be observed for bare Li metal anode after only 150 h due to the heterogeneous Li deposition and the serious side reaction between electrolyte and Li metal (Figure 4a). Benefiting from the conductive 3D nickel network, which could not only reduce the local current density and hence relieve the growth of Li

Research Article
doi.org/10.1002/batt.202100408
Chemistry Europe
European Chemical Societies Publishing

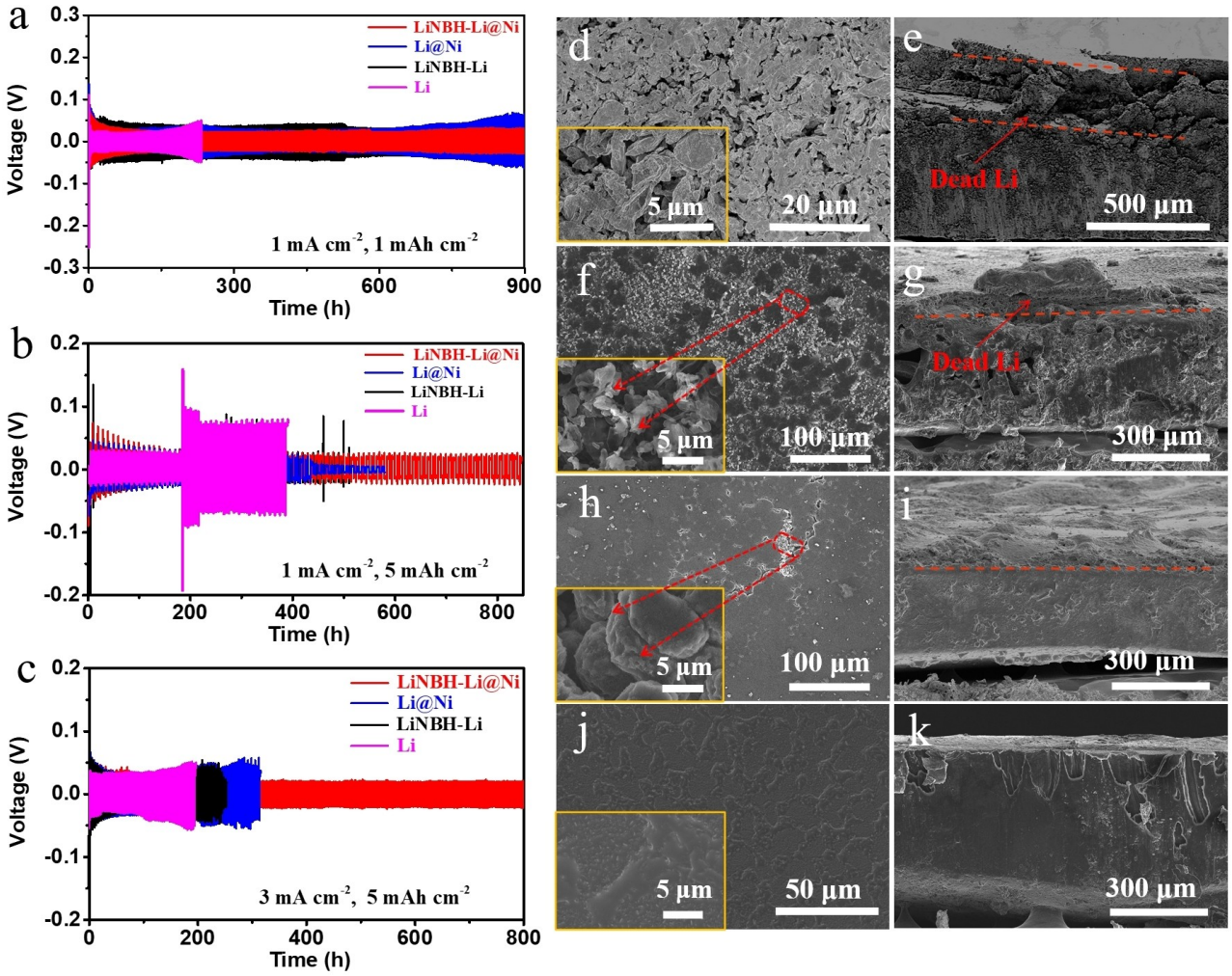

Figure 4. a–c) Galvanostatic discharge/charge voltage profiles of LiNBH-Li@Ni, Li@Ni, LiNBH-Li, and bare Li in symmetrical cells at various current densities with different areal capacities area capacities. Top-view and cross-sectional SEM images of d, e) bare Li metal, f, g) Li@Ni, h, i) LiNBH-Li and j, k) LiNBH-Li@Ni electrodes, respectively, after 50 cycles at 1 mA cm^{-2} with a fixed capacity of 3 mAh cm^{-2} in symmetrical cells.

dendrites but also accommodate the volume change of Li metal upon repeated Li stripping and plating process,[35] the Li@Ni electrode exhibits a stable cycling performance over 650 h with an overpotential of 31 mV. However, owing to the inevitable reaction between electrolyte with Li metal on the top surface of the electrode, the continuous increase of overpotential to 57 mV could be observed for Li@Ni electrode after 850 h (Figure S5a).[36] In strong contrast, the LiNBH-Li@Ni electrode, as well as pristine Li metal covered with $[LiNBH]_n$ layer (denoted as LiNBH-Li), displays a low average overpotential of ~27 mV for over 900 h, indicating that the $[LiNBH]_n$ layer is able to guide uniform Li nucleation and protect Li metal from the erosion of electrolyte (Figure S5b). In addition, the nucleation overpotential for Li plating, defined as the gap between the bottom of the voltage dip and the subsequent voltage plateau, is investigated upon discharging at 1 mA cm^{-2} (Figure S6). The deposition of Li metal on bare Li metal has an obvious nucleation overpotential of 96 mV, whereas this value could be significantly decreased to 37 mV and 13 mV for Li@Ni and LiNBH-Li@Ni, respectively. This result indicates the synergistic role of the electronic conductive 3D Ni foams as the hosts and the $[LiNBH]_n$ layers with high Li ion conductivity as the protective roof in reducing the nucleation barrier of Li.[17,18,37] Upon increasing the Li plating capacity to 5 mAh cm^{-2} (Figure 4b), the bare Li metal electrode, as expected, suffers a huge sudden elevation of overpotential after only 180 h and the cycling life of the Li@Ni electrode could be extended to 440 h owing to the presence of the conductive 3D Ni foams as the host. After that, a sharp decrease of voltage appears suddenly for the Li@Ni electrode (Figure S7a), indicating the internal short circuit of the cell due to the inevitable growth of Li dendrites that could pierce the separator. Interestingly, although the steady overpotential of LiNBH-Li electrode could be maintained at the initial 300 h, an abrupt voltage increase after major fluctuation happens again upon cycling for 460 h (Figure S7b), which could be mainly attributed to the continuous break of $[LiNBH]_n$ artificial protective layer induced by the large volume expansion of Li metal .[36] By comparison, induced by the synergistic role of the conductive 3D Ni foams and $[LiNBH]_n$ as the artificial protective layer, the LiNBH-Li@Ni anode

displays a stable overpotential of ~18 mV for over 850 h. When the current density is increased to 3 mA cm^{-2} (Figure 4c), the LiNBH-Li@Ni anode can still deliver a stable long-term cycling performance with a smooth voltage plateau for 800 h, much superior to that of Li@Ni, LiNBH-Li, and bare Li electrodes, respectively. Impressively, the LiNBH-Li@Ni electrode is capable of operating stably for over 350 h under an ultrahigh current density of 10 mA cm^{-2} with a high areal capacity of 5 mAh cm^{-2} (Figure S8), which provides further evidence to the capability of LiNBH-Li@Ni in effectively improving the cycling stability of Li plating and stripping process.

To better understand the mechanism for the excellent cycling stability of the LiNBH-Li@Ni anode, the exchange current density and electrochemical impedance spectroscopy (EIS) are conducted on the symmetric cells upon cycling. After 50 cycles of Li stripping and plating process at 1 mA cm^{-2} with a capacity of 3 mAh cm^{-2}, the Tafel profile obtained from cyclic voltammetry measurements shows that the exchange current density of the LiNBH-Li@Ni electrode is approximately 2.32 mA cm^{-2} (Figure S9), much higher than that of both LiNBH-Li electrode (~2.13 mA cm^{-2}) and Li@Ni electrode (~1.13 mA cm^{-2}), indicating that the modification of $[LiNBH]_n$ on the surface of Li@Ni anode could effectively enhance the both charge-transfer kinetic and Li ion transportation kinetics of the whole electrode.[38] According to the EIS results (Figure S10 and Table S1), the charge-transfer resistance (R_{ct}) of the LiNBH-Li@Ni electrode in symmetric cell after 50 cycles could be calculated to be approximately 4.64 Ω, much lower than that of LiNBH-Li (i.e., 9.61 Ω) and Li@Ni (i.e., 10.58 Ω), respectively, indicating the superior cycling stability of the LiNBH-Li@Ni electrode with high electronic and ionic conductivity.[39] SEM images illustrate that, after 50 cycles of Li stripping and plating process, a completely loose layer of "dead Li" composed of large amounts of cracks and Li dendrites with a thickness of nearly 160 μm is formed on the surface of bare Li foil (Figure 4d and e). Taking advantage of the confinement role of the conductive 3D Ni foams, the surface of the Li@Ni electrode after cycling is denser compared with bare Li metal (Figure 4f). Nevertheless, some bunchy Li dendrites could still be observed from the enlarged SEM image with the formation of partial "dead Li" as verified by the cross-sectional observation (Figure 4g). Moreover, although the LiNBH-Li electrode exhibits a flat and tight surface under the protection of $[LiNBH]_n$ layer after 50 cycles, a few small cracks, in which Li particles randomly pile up, are present on the top surface of the electrode (Figure 4h). It is capable of breaking up the artificial layer upon cycling, eventually leading to the growth of "dead Li" and the pulverization of Li metal anode (Figure 4i). By comparison, the LiNBH-Li@Ni anode displays a relatively smooth and dense surface without the observation of any Li dendrites (Figure 4j and k), which is comparable to the morphology of the freshly fabricated electrode. This sharp contrast directly confirms the excellent stability of the as-prepared LiNBH-Li@Ni electrode towards dendrite-free cycling performance.

To investigate the stability and reversibility of the LiNBH-Li@Ni anode applied in practical application, full cells coupled with commercial $LiFePO_4$ (LFP) cathode are assembled and tested. As shown in Figure 5(a), the assembled LiNBH-Li@Ni// LFP full cell exhibits a reversible capacity of 112.1 mAh g^{-1} at 1 C (1 C = 170 mA g^{-1}) after over 800 cycles, corresponding to a capacity retention of 84.5%. By comparison, an obvious decay of the reversible capacity to be 99.7 mAh g^{-1}, corresponding to a capacity retention of 73.5%, could be observed for the Li// LFP full cell after only 458 cycles. Moreover, the LiNBH-Li@Ni// LFP full cell delivers a better rate performance than that of Li// LFP full cell (Figure 5b). Particularly, the LiNBH-Li@Ni//LFP full cell delivers a high reversible capacity of 110.5 and 102.2 mAh g^{-1} at 2 C and 3 C, respectively, and this value recovers to 140.2 mAh g^{-1} when the current density returns to 0.5 C, indicating the excellent reversibility of LiNBH-Li@Ni//LFP full cell. In contrast, the reversible capacity rapidly decays to only 101.2 and 84.5 mAh g^{-1} at 2 C and 3 C, respectively, for Li// LFP full cell. In addition, the LiNBH-Li@Ni//LFP full cell displays a much smaller polarization in the charge and discharge process than that of Li//LFP full cell during the whole cycling process (Figure S13), indicating fast charge-transfer kinetics at the interface between the LiNBH-Li@Ni anode and electrolyte. This result could be further supported by the significant decrease of R_{ct} of LiNBH-Li@Ni//LFP full cell (i.e., 58.4 Ω) in comparison with that of Li//LFP full cell (i.e., 127.7 Ω) after 80 cycles (Figure 5c). Furthermore, the areal mass loading of the LFP cathode in the LiNBH-Li@Ni//LFP full cell is increased to 12 mg cm^{-2} for investigation. Impressively, the LiNBH-Li@Ni// LFP full cell delivers a high reversible capacity of 141.2 mAh g^{-1} at 0.5 C after over 130 cycles (Figure S14a) and 127.4 mAh g^{-1} at 1 C after over 200 cycles (Figure 5d), respectively, with the corresponding coulombic efficiencies approaching 100% (Figures S14b and S15). By comparison, the Li//LFP full cell suffers from a severe capacity decay after only 147 cycles under identical condition. As expected, the rate performance of LiNBH-Li@Ni//LFP full cell is still superior to that of Li//LFP full cell upon increasing the areal mass loading of the LFP cathode (Figure 5e).

Conclusion

In summary, a novel "house strategy" that combines Ni foam modified with NiO nanosheets as the conductive host to confine Li metal and $[LiNBH]_n$ polymer with high ionic conductivity as the protective roof is developed to not only suppress the growth of Li dendrites but also alleviate the infinite volume change of Li-metal anode. Owing to the synergistic effect of NiO/Ni foam with large specific surface area and high Li reservoir that could effectively accommodate the volume change and lower the local current density and the $[LiNBH]_n$ protective layer that could promote a uniform Li^+ flux and regulate the Li homogeneously deposit, the thus-formed LiNBH-Li@Ni electrode presents an outstanding cycling stability. In symmetric cells, the LiNBH-Li@Ni electrode could maintain a stable cycling performance for over 800 h with a high cyclic capacity of 5 mAh cm^{-2} at 3 mA cm^{-2}. When coupled with $LiFePO_4$ cathode (the area loading is 12 mg cm^{-2}), an ultrahigh reversible capacity of 127.4 mAh g^{-1} could be achieved in

Research Article
doi.org/10.1002/batt.202100408
Chemistry Europe
European Chemical Societies Publishing

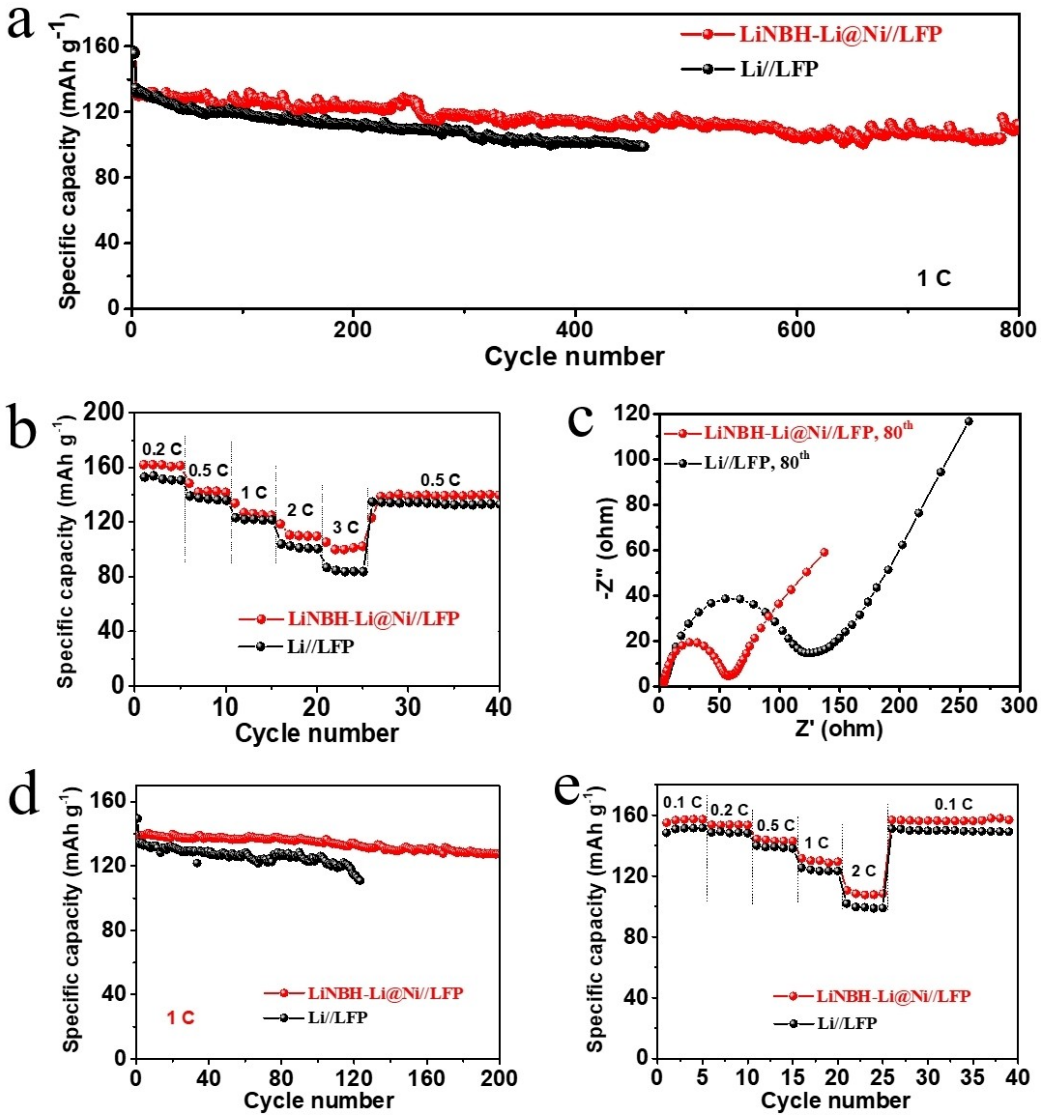

Figure 5. a) Cycling performance of LiNBH-Li@Ni//LFP, and Li//LFP full cells at 1 C (1 C = 170 mA g^{-1}). b) Rate capability of LiNBH-Li@Ni//LFP, and Li//LFP full cells, in which the areal mass loading of the LFP cathode is controlled to be approximately 3 mg cm^{-2}. c) The electrochemical impedance spectra of LiNBH-Li@Ni//LFP and Li//LFP full cells after 80 cycles. d) Cycling performance of LiNBH-Li@Ni//LFP and Li//LFP full cells at 1 C, in which the areal mass loading of the LFP cathode is controlled to be approximately 12 mg cm^{-2}. e) Rate capability of LiNBH-Li@Ni//LFP and Li//LFP full cells.

LiNBH-Li@Ni//LFP full cell at 1 C after 200 cycles. This strategy opens new doors for designing dendrite-free and high-stability Li-metal anode.

Supporting Information

Supporting Information is available from the Wiley Online Library or from the author.

Acknowledgements

This work was partially supported by the National Science Fund for Distinguished Young Scholars (51625102), the National Natural Science Foundation of China (51971065, 51901045, U2130208, U1903217, 21978073), the Innovation Program of Shanghai Municipal Education Commission (2019-01-07-00-07-E00028), the Science and Technology Commission of Shanghai Municipality (No. 21ZR1407500), and the Programs for Professor of Special Appointment (Eastern Scholar) at Shanghai Institutions of Higher Learning.

Conflict of Interest

The authors declare no conflict of interest.

Data Availability Statement

The data that support the findings of this study are available in the supplementary material of this article.

Keywords: 3D NiO/Ni foam · house strategy · Li metal anodes · $[LiNBH]_n$ protective layer

[1] D. Lin, Y. Liu, Y. Cui, *Nat. Nanotechnol.* **2017**, *12*, 194.
[2] W. Xu, J.-L. Wang, F. Ding, X.-L. Chen, E. Nasybulin, Y.-H. Zhang, J.-G. Zhang, *Energy Environ. Sci.* **2014**, *7*, 513.
[3] D. Aurbach, E. Zinigrad, Y. Cohen, H. Teller, *Solid State Ionics* **2002**, *148*, 405.
[4] K. J. Harry, D. T. Hallinan, D. Y. Parkinson, A. A. MacDowell, N. P. Balsara, *Nat. Mater.* **2014**, *13*, 69.
[5] J. Liu, Z. Bao, Y. Cui, E. J. Dufek, J. B. Goodenough, P. Khalifah, Q. Li, B. Y. Liaw, P. Liu, A. Manthiram, Y.-S. Meng, V. R. Subramanian, F. T. Michael, V. V. Viswanathan, M. S. Whittingham, J. Xiao, W. Xu, J. Yang, X.-Q. Yang, J.-G. Zhang, *Nat. Energy* **2019**, *4*, 180.
[6] X.-B. Cheng, R. Zhang, C.-Z. Zhao, Q. Zhang, *Chem. Rev.* **2017**, *117*, 10403.
[7] Y. Li, Y. Li, A. Pei, K. Yan, Y. Sun, C.-L. Wu, L. M. Joubert, R. Chin, A. L. Koh, Y. Yu, J. Perrino, B. Butz, S. Chu, Y. Cui, *Science* **2017**, *358*, 506.
[8] K. Yan, J. Wang, S. Zhao, D. Zhou, B. Sun, Y. Cui, G. Wang, *Angew. Chem. Int. Ed.* **2019**, *131*, 11486.
[9] H. Zhang, G. G. Eshetu, X. Judez, C. Li, L. M. Rodriguez-Martinez, M. Armand, *Angew. Chem. Int. Ed.* **2018**, *57*, 15002.
[10] H. Chen, A. Pei, D. Lin, J. Xie, A. Yang, J. Xu, K. Lin, J. Wang, H. Wang, F. Shi, D. Boyle, Y. Cui, *Adv. Energy Mater.* **2019**, *9*, 1900858.
[11] Q. Pang, X. Liang, I. R. Kochetkov, P. Hartmann, L. F. Nazar, *Angew. Chem. Int. Ed.* **2018**, *130*, 9943.
[12] Y. Gao, Z. Yan, J. L. Gray, X. He, D. Wang, T. Chen, Q. Huang, Y.-C. Li, H. Wang, S. H. Kim, T. E. Malouk, D. Wang, *Nat. Mater.* **2019**, *18*, 384.
[13] Z. Jiang, L. Jin, Z. Han, W. Hu, Z. Zeng, Y. Sun, J. Xie, *Angew. Chem. Int. Ed.* **2019**, *58*, 11374.
[14] F.-F. Liu, L.-F. Wang, Z.-W. Zhang, P.-C. Shi, Y.-Z. Feng, Y. Yao, S.-F. Ye, H.-Y. Wang, X.-J. Wu, Y. Yu, *Adv. Funct. Mater.* **2020**, *30*, 2001607.
[15] Y.-X. Yao, X.-Q. Zhang, B.-Q. Li, C. Yan, P.-Y. Chen, J.-Q. Huang, Q. Zhang, *InfoMat* **2020**, *2*, 379.
[16] Z.-J. Wang, Y.-Y. Wang, Z.-H. Zhang, X.-W. Chen, W. Lie, Y.-B. He, Z. Zhou, G.-L. Xia, Z. P. Guo, *Adv. Funct. Mater.* **2020**, *30*, 2002414.
[17] G.-X. Huang, S.-R. Chen, P.-M. Guo, R.-M. Tao, K.-C. Jie, B. Liu, X.-F. Zhang, J.-Y. Liang, Y.-C. Cao, *Chem. Eng. J.* **2020**, *395*, 125122.
[18] J.-F. Zhu, J. Chen, Y. Luo, S.-Q. Sun, L.-G. Qin, H. Xu, P.-G. Zhang, W. Zhang, W.-B. Tian, Z.-M. Sun, *Energy Storage Mater.* **2019**, *23*, 539.
[19] X.-Y. Yue, W.-W. Wang, Q.-C. Wang, J.-K. Meng, Z.-Q. Zhang, X.-J. Wu, X.-Q. Yang, Y.-N. Zhou, *Energy Storage Mater.* **2018**, *14*, 335.
[20] L. Yu, N. L. Canfield, S. R. Chen, H. Lee, X.-D. Ren, M. H. Engelhard, Q.-Y. Li, J. Liu, W. Xu, J.-G. Zhang, *ChemElectroChem* **2018**, *5*, 761.
[21] M. Lei, Z. You, L. Ren, X. Liu, J.-G. Wang, *J. Power Sources* **2020**, *463*, 228191.
[22] M. Lei, J.-G. Wang, L. Ren, D. Nan, C. Shen, K. Xie, X.-R. Liu, *ACS Appl. Mater. Interfaces* **2019**, *11*, 30992.
[23] Y.-S. He, M.-J. Li, Y.-G. Zhang, Z.-Z. Shan, Y. Zhao, J.-D. Li, G.-H. Liu, C.-Y. Liang, Z. Bakenov, Q. Li, *Adv. Funct. Mater.* **2020**, *30*, 2000613.
[24] P.-B. Zhai, T.-S. Wang, H.-N. Jiang, J.-Y. Wan, Y. Wei, L. Wang, W. Liu, Q. Chen, W.-W. Yang, Y. Cui, Y.-J. Gong, *Adv. Mater.* **2021**, *33*, 2006247.
[25] K. Lin, X.-Y. Qin, M. Liu, X.-F. Xu, G.-M. Liang, J.-X. Wu, F.-Y. Kang, G.-H. Chen, B.-H. Li, *Adv. Funct. Mater.* **2019**, *29*, 1903229.
[26] C. Niu, H. Pan, W. Xu, J. Xiao, J.-G. Zhang, L. Luo, C. Wang, D. Mei, J. Meng, X. Wang, Z. Liu, L. Mai, J. Liu, *Nat. Nanotechnol.* **2019**, *14*, 594.
[27] Y. Xu, T. Li, L. Wang, Y. Kang, *Adv. Mater.* **2019**, *31*, 1901662.
[28] S.-S. Chi, Y.-C. Liu, W.-L. Song, L.-Z. Fan, Q. Zhang, *Adv. Funct. Mater.* **2017**, *27*, 1700348.
[29] Q. Zhang, W.-L. Bai, C.-Y. Sun, X. Liu, K.-X. Wang, J.-S. Chen, *Chem. Eng. J.* **2021**, *405*, 127022.
[30] S. Frueh, R. Kellett, C. Mallery, T. Molter, W. S. Willis, C. King'ondu, S. L. Suib, *Inorg. Chem.* **2011**, *50*, 783.
[31] G.-L. Xia, J. Chen, W.-W. Sun, Y.-B. Tan, Z.-P. Guo, H.-K. Liu, X.-B. Yu, *Nanoscale* **2014**, *6*, 12333.
[32] R. Chiriac, F. Toche, U. B. Demirci, O. Krol, P. Miele, *Int. J. Hydrog. Energy* **2011**, *36*, 12955.
[33] B. Han, D.-Y. Feng, S. Li, Z. Zhang, Y.-C. Zou, M. Gu, H. Meng, C.-Y. Wang, K. Xu, Y.-S. Zhao, H.-B. Zeng, C.-S. Wang, Y.-H. Deng, *Nano Lett.* **2020**, *20*, 4029.
[34] W. Liu, D. Lin, A. Pei, Y. Cui, *J. Am. Chem. Soc.* **2016**, *138*, 15443.
[35] H. J. S. Sand, *Philos. Mag.* **1901**, *1*, 45.
[36] Y.-Y. Feng, C.-F. Zhang, B. Li, S.-Z. Xiong, J.-X. Song, *J. Mater. Chem. A* **2019**, *7*, 6090.
[37] H. Liu, J.-G. Wang, W. Hua, H. Sun, H. Yu, S. Tian, Z. Hou, J. Yang, C. Wei, F. Kang, *Adv. Sci.* **2021**, *8*, 2102612.
[38] S.-F. Ye, L.-F. Wang, F.-F. Liu, P.-C. Shi, H.-Y. Wang, X.-J. Wu, Y. Yu, *Adv. Energy Mater.* **2020**, *44*, 2002647.
[39] S.-F. Liu, X.-H. Xia, Z.-J. Yao, J.-B. Wu, L.-Y. Zhang, S.-J. Deng, C.-G. Zhou, S.-H. Shen, X.-L. Wang, J.-P. Tu, *Small Methods* **2018**, *2*, 1800035.

Manuscript received: December 22, 2021
Revised manuscript received: January 26, 2022
Version of record online: March 4, 2022